ORIGINAL ARTICLE

Volume 20 Issue 2 2025

DOI: 10.21315/aos2025.2002.OA01

ARTICLE INFO

Submitted: 20/11/2024
Accepted: 20/08/2025
Online: 22/12/2025

Physicochemical Characterisation and Biocompatibility of Bioactive Glass/ Polycaprolactone Scaffold for Alveolar Bone Regeneration

Ain Nurfatehah Arupudin[a], Ahmad Hazim Norafizal[a], Farha Ariffin[b], Siti Noor Fazliah Mohd Noor[c], Nurul Aida Ngah[d]*

[a]*Faculty of Dentistry, Universiti Teknologi MARA, 47000 Sungai Buloh, Selangor, Malaysia*

[b]*Centre of Studies for Periodontology, Faculty of Dentistry, Universiti Teknologi MARA, 47000 Sungai Buloh, Selangor, Malaysia*

[c]*Biomaterials Group, Oral Cancer Research Program, Advanced Medical and Dental Institute, Universiti Sains Malaysia, 13200 Kepala Batas, Pulau Pinang, Malaysia*

[d]*Centre of Studies for Oral and Maxillofacial Surgery, Faculty of Dentistry, Universiti Teknologi MARA, 47000 Sungai Buloh, Selangor, Malaysia*

*Corresponding author: dr.aidangah@uitm.edu.my

To cite this article: Arupudin AN, Norafizal AH, Ariffin F, Noor SNFM, Ngah NA (2025). Physicochemical characterisation and biocompatibility of bioactive glass/polycaprolactone scaffold for alveolar bone regeneration. *Arch Orofac Sci*, **20**(2): 111–124. https://doi.org/10.21315/aos2025.2002.OA01

To link to this article: https://doi.org/10.21315/aos2025.2002.OA01

ABSTRACT

In bone tissue engineering, scaffold-based approaches offer great potential for regenerating damaged or lost bone tissue. Composite scaffolds have gained popularity because they combine the beneficial properties of two or more materials, providing promising biomimetic properties for tissue regeneration. In our study, combining the biocompatibility of bioactive glass with the mechanical qualities of polycaprolactone provides tailored properties and scaffold architecture conducive to alveolar bone regeneration. This study aims to develop a bone substitute using bioactive glass/polycaprolactone (BG/PCL) composites and to evaluate its biocompatibility for potential applications in alveolar bone regeneration. BG/PCL scaffolds were fabricated using a solvent-casting method at three different weight percentages (wt.%) ratios (10:90, 20:80, and 30:70). The scaffolds were characterised using scanning electron microscopy (SEM), Fourier transform infrared (FTIR) spectroscopy, and methyl tetrazolium (MTT) (3-(4,5-Dimethylthiazol-2-yl)-2,5-Diphenyltetrazolium Bromide) Assay to evaluate their physical, chemical, and biocompatibility properties. Among the three BG:PCL composite ratios tested (10:90, 20:80, and 30:70), the 10:90 ratio demonstrated the most favourable properties. SEM analysis of this composition revealed optimal surface roughness and well-distributed interconnected pores, which are conducive to cell attachment, enhanced cellular infiltration, and efficient nutrient diffusion. FTIR spectra displayed characteristic absorption bands corresponding to the functional groups of BG and PCL components while the biocompatibility test confirmed the viability and proliferation of

 ©Penerbit Universiti Sains Malaysia. 2025
This work is licensed under the terms of the Creative Commons Attribution (CC BY) (http://creativecommons.org/licenses/by/4.0/).

periodontal ligament (PDL) fibroblast cells when cultured with the scaffolds. This study demonstrates that the developed BG/PCL composite, especially at the 10:90 ratio, possesses suitable properties and biocompatibility, highlighting its potential for use in alveolar bone regeneration.

Keywords: *Alveolar bone regeneration; bioactive glass; composite scaffold; polycaprolactone*

INTRODUCTION

Maxillofacial bone deformities can be caused by a wide range of conditions, including infections, trauma, periodontal disease, oral cancer, tooth extractions, and other dental issues. It differs by socioeconomic level, cultural traits, geographical region, and among various age groups (Wusiman *et al.*, 2020). These bone defects have a negative impact on facial aesthetics and crucial oral functions like mastication, speaking, and feeding, which dramatically lowers patient quality of life. Thus, it is significant to develop the most effective regenerative treatment for the injuries happening in this area to prevent their potential to cause permanent alveolar bone defects.

Additionally, a variety of illnesses, conditions, and injuries can result in alveolar bone abnormalities in the maxillofacial region. It might develop from systemic factors, such as congenital anomalies, general diseases, and drugs. It can also happen because of local factors, such as inflammation, traumatic injuries from accidents or surgical procedures. Alveolar bone defects could also result from dental procedures like tooth extractions as well as surgical procedures, such as the removal of malignant or benign tumours. Surgically removed malignant tumours of the oral cavity are frequently treated with additional therapies like immunotherapy, chemotherapy, or radiotherapy. The surgical resection procedure could lead to significant tissue loss and leave large residual bone defects in the affected region (Muzaffar *et al.*, 2021). Additionally, alveolar bone deficiencies may result from several reasons, including craniomaxillofacial trauma resulting from motor vehicular collisions, falls, and other accidents (Manodh *et al.*, 2016).

Unfortunately, the optimum method and material for alveolar bone regeneration have not yet been fabricated and until now, autologous bone grafting from iliac bone remains the standard of choice for alveolar bone reconstruction. However, it is linked to several complications, including gait difficulties, infection, nerve damage, persistent discomfort, and prolonged hospitalisation to the patients. Consequently, bone tissue engineering has emerged as a promising alternative, leveraging scaffolds, cells, and bioactive molecules to facilitate regeneration (Larsson *et al.*, 2016).

A bone scaffold is a three-dimensional matrix that facilitates the adherence and growth of osteogenic cells, capable of guiding bone growth and stimulating new bone formation (Ghassemi *et al.*, 2018). Scaffolds serve as critical templates for bone regeneration, providing structural support and a conducive microenvironment for cell adhesion, proliferation, and differentiation (Yousefiasl *et al.*, 2023). Ideal scaffolds require biocompatibility, biodegradability, and mechanical stability, necessitating careful selection of biomaterials. Among available options, bioactive glass (BG) exhibits exceptional osteoconductivity, bioactivity, and antibacterial properties, promoting hydroxyapatite formation and stimulating osteogenesis (Granel *et al.*, 2019). However, its brittleness limits standalone use. Conversely, polycaprolactone (PCL), an FDA-approved synthetic polymer, offers tunable degradation kinetics, flexibility, and biocompatibility, making it suitable for load-

bearing applications (Kundu *et al.*, 2015; Darie-Niță *et al.*, 2022). Combining BG with PCL may synergise their strengths, enhancing mechanical resilience while maintaining bioactivity.

In tissue engineering, along with the biomaterials scaffold, cells are crucial components for tissue regeneration. Human periodontal ligament fibroblasts (HPLFs) are mesenchymal-derived fibroblasts that are found in the periodontal ligament (PDL) that surrounds the tooth root. HPLFs play a pivotal role in periodontal and alveolar bone regeneration due to their high proliferative capacity and ability to remodel surrounding tissue (Nanci & Bosshardt, 2006).

This study aims to develop a bone substitute using BG/PCL composites and to evaluate its biocompatibility for potential applications in alveolar bone regeneration. This innovative approach could address limitations of current grafts, offering a viable alternative for alveolar bone regeneration.

MATERIAL AND METHODS

Scaffold Fabrication and Characterisation

BG was obtained from Universiti Sains Malaysia and biodegradable PCL with molecular weight 80,000g/mol, were purchased from Sigma-Aldrich, UK. To ensure homogeneity, PCL was dissolved in 5% chloroform (w/v), mixed with BG powder, and processed using a sonicator (Ufere & Sultana, 2016). Ratios of 10:90, 20:80, and 30:70 were chosen based on established protocols reflecting alveolar bone density (Lu *et al.*, 2014). The prepared BG/PCL mixture was then placed into a separated mould and left under fume hood at room temperature for 24 hours to allow evaporation of the chloroform. Eventually, thin membrane films obtained were air-dried for further 24 hours and placed inside desiccators to avoid material degradation (Kuo *et al.*, 2021) (Fig. 1).

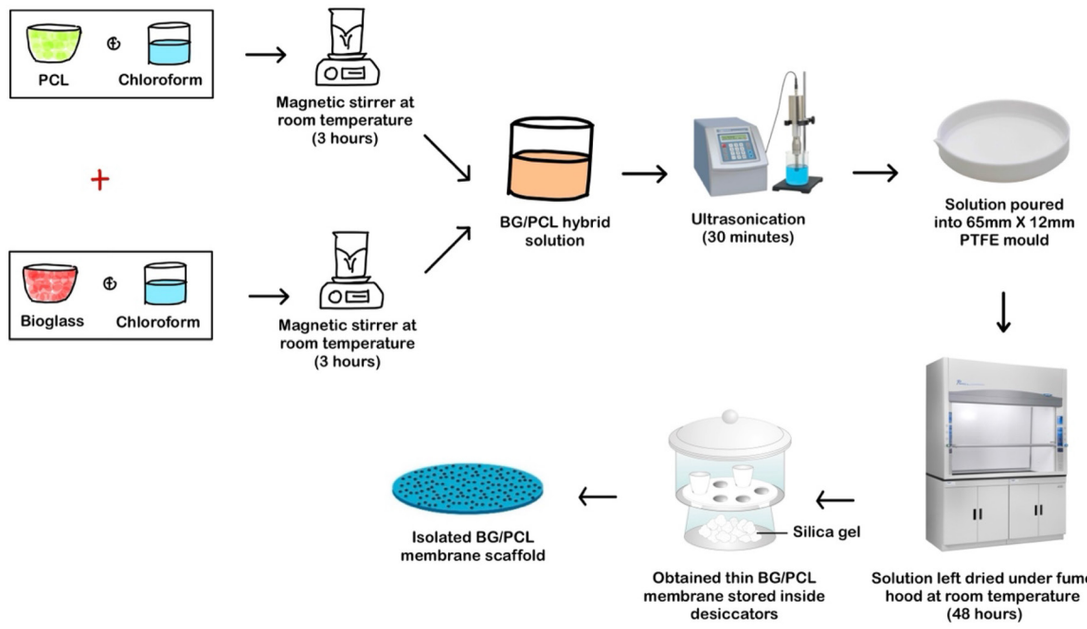

Fig. 1 Fabrication steps of BG/PCL membrane scaffold via sonication and solvent casting.

Scanning electron microscopy (SEM) was employed using the Hitachi TM3000, following sputter coating with gold/palladium to improve conductivity. Images were obtained at different magnifications and processed using ImageJ to assess particle size and surface roughness (Malagón-Escandón *et al.*, 2021). Additionally, Fourier transform infrared (FTIR) spectroscopy was done to analyse molecular vibrations and chemical bonds within the scaffolds. The interpretation of peaks and patterns allowed for the identification of specific functional groups and chemical components.

Cell Culture Techniques and Analysis

HPLFs were cultured to assess the biocompatibility of the BG/PCL scaffold. Cells were maintained in T75 flasks with Dulbecco's Modified Eagle's Medium (DMEM) supplemented with 10% fetal bovine serum (FBS) at 37°C and 5% CO_2 until 80% confluency. For subculture, adherent cells were washed with PBS, detached using trypsin-EDTA, neutralised with fresh medium, and centrifuged. The cell pellet was resuspended in DMEM, and cell density was determined using a hemocytometer.

Prior to cell seeding, scaffolds were sterilised and pre-conditioned in DMEM (30 min, 37°C). A density of 10,000 HPLFs per well was seeded onto scaffolds in 96-well plates, with scaffold-only wells serving as controls. Seeded constructs were incubated for 72 hours.

Cell viability was evaluated via methyl tetrazolium (MTT) assay. After incubation, medium was replaced with MTT solution (5 mg/mL, 4 hours), and formazan crystals were dissolved with dimethyl sulfonic oxide (DMSO) solution and discarded after 30 minutes. Absorbance was measured at 570 nm using a microplate reader to detect the optical density at 570 nm (Safi *et al.*, 2020).

For morphological analysis, cell-seeded scaffolds and controls were washed in PBS, fixed in 4% glutaraldehyde (1–2 hours), and a gradual dehydration process using a series of ethanol washes were performed (Abay *et al.*, 2019). Samples were then imaged via SEM to examine cell adhesion and surface morphological microstructure.

RESULTS

Scanning Electron Microscopy

The fabricated BG/PCL composite scaffolds displayed uniform dimensions, with all groups measuring the same diameter (Fig. 2). However, slight variations in average weight were noted relative to BG concentrations (Table 1).

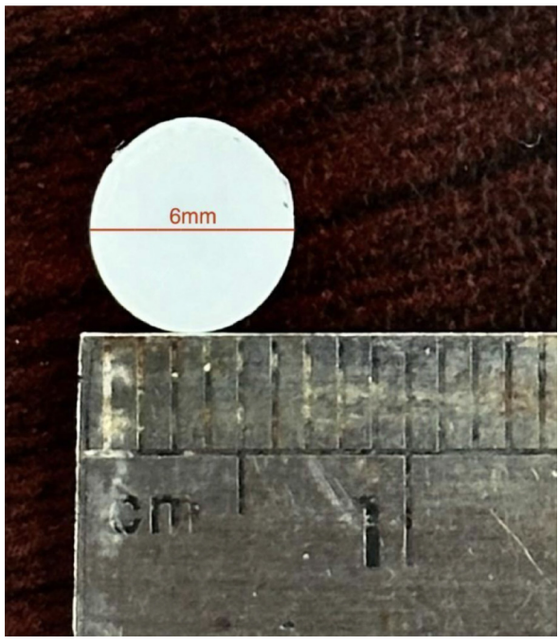

Fig. 2 Representative image displaying fabricated BG/PCL scaffolds captured by the authors. The scaffold is round with a diameter of 6 mm.

Table 1 Diameter and mean weight of fabricated BG/PCL scaffold from three different compositions

BG/PCL composition	Diameter/mm	Mean weight/mg (n = 20)
10:90	6.0	21.60
20:80	6.0	21.13
30:70	6.0	19.7

Surface roughness and morphological features characterisation were conducted on three different compositions of bone scaffolds: 10:90 BG/PCL, 20:80 BG/PCL, and 30:70 BG/PCL. SEM images revealed distinct differences in surface morphology among the samples at both 500 and 1,500 magnifications (Fig. 3).

The 10:90 BG/PCL scaffold exhibited the most pronounced surface roughness among the three compositions with a highly irregular and textured surface, characterised by numerous protrusions and valleys (Fig. 3A). The 20:80 BG/PCL scaffold revealed a moderately irregular surface with fewer prominent features compared to the 10:90 BG/PCL scaffold but was still notably rougher than the 30:70 BG/PCL scaffold (Fig. 3B). In contrast, the 30:70 BG/PCL scaffold exhibited the least surface roughness among all compositions. SEM analysis of 30:70 BG/PCL scaffold showed a relatively smooth and uniform surface texture, with minimal irregularities or protrusions observed at both magnifications (Fig. 3C).

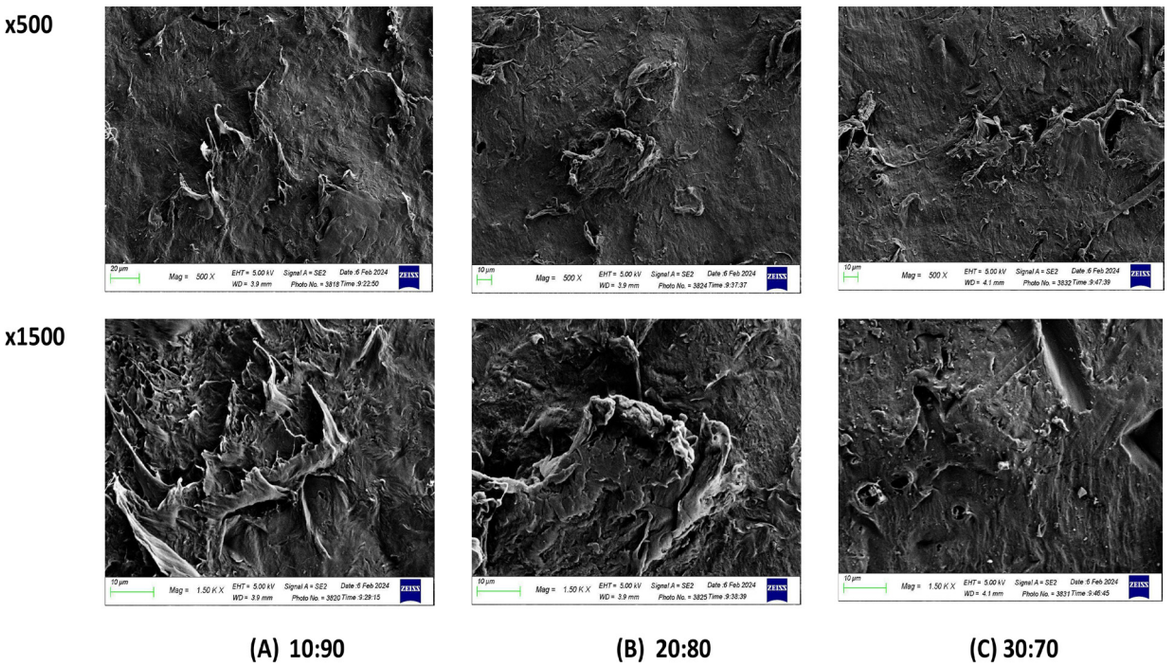

Fig. 3 Representative SEM images displaying surface morphology of BG/PCL scaffolds captured at two different magnifications: 500× and 1,500×. (A) represents 10:90; (B) represents 20:80; and (C) represents 30:70 weight percentages (wt.%) ratio of the BG/PCL scaffold.

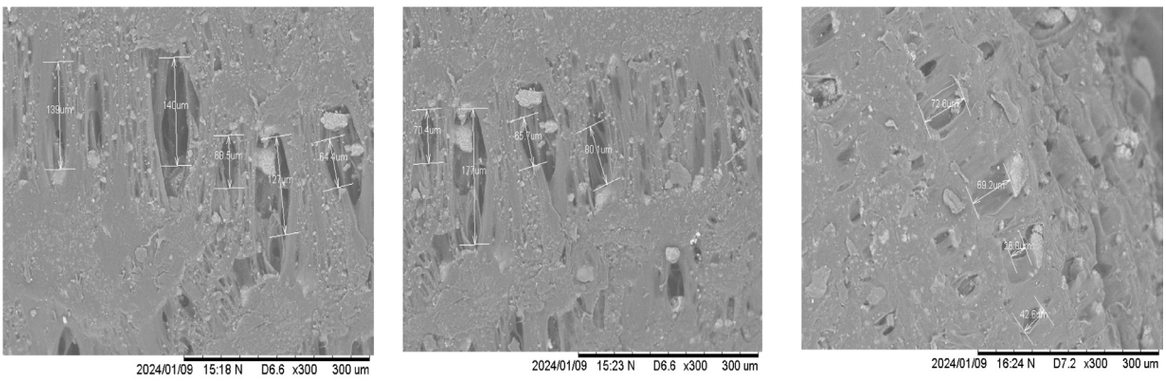

(A) 10:90 **(B) 20:80** **(C) 30:70**

Fig. 4 Representative SEM images displaying characterisation of porosity present on BG/PCL scaffolds captured at 300× magnification. (A) represents 10:90 BG/PCL scaffold; (B) represents 20:80 BG/PCL scaffold; and (C) represents 30:70 BG/PCL scaffold.

The 10:90 BG/PCL composition exhibited the largest and most interconnected pores, with a mean pore size of 102.29 μm, facilitating potential nutrient diffusion and cell infiltration (Table 2). The pores appeared well-defined and uniformly distributed, with some larger void spaces interspersed among smaller pores (Fig. 4A).

The 20:80 BG/PCL scaffold displayed a moderately porous structure with a mean pore size of 96.6 μm (Fig. 4B), whereas the 30:70 BG/PCL scaffold had the lowest porosity with a mean pore size of 87.8 μm with regions of dense polymer matrix dominating the scaffold architecture (Fig. 4C).

Table 2 Mean pore sizes on different groups of BG/PCL scaffolds

BG/PCL composition	Mean pore sizes/ μm
10:90	102.295
20:80	96.619
30:70	87.840

The analysis of cell morphology reveals distinct characteristics of HPLFs cultured on the different groups of BG/PCL composite scaffolds. Microscopic examination under 500×, 1,500× and 8,000× magnification reveals a heterogeneous population of HPLFs exhibiting diverse shapes and structures (Fig. 5). Numerous clusters of cells were noted under 500× magnification, and more clearly in the higher magnification of 1,500× and 8,000×. While a significant proportion of cells exhibit elongated and spindle-shaped morphologies (Fig. 5B) with well-defined cytoplasmic extensions, others present in a nodular configuration, suggesting the presence of cell aggregates or clusters (Fig. 5A, 5C).

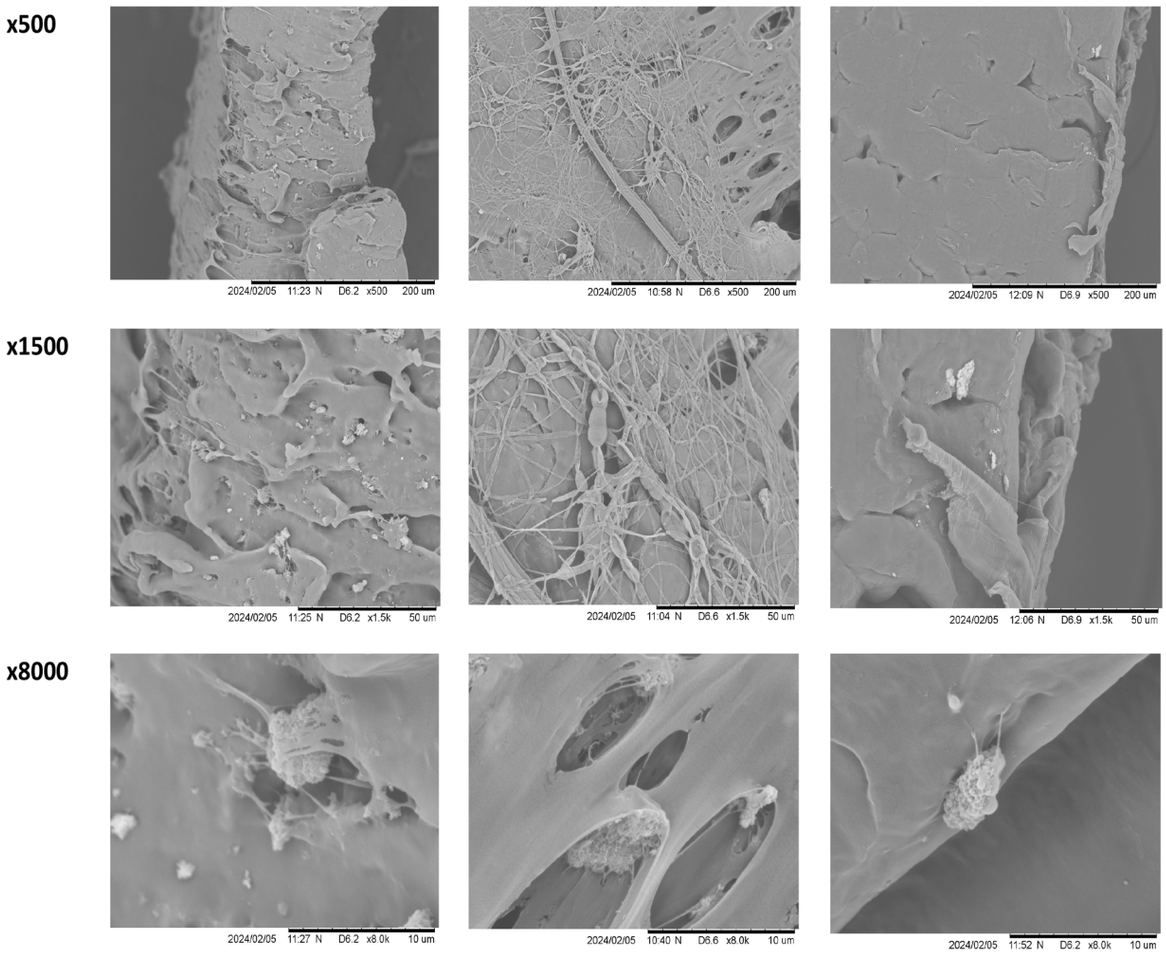

Fig. 5 Representative SEM images displaying cell structure present on BG/PCL scaffolds captured at three different magnifications: 500×, 1500× and 8000×. (A) represents 10:90 BG/PCL scaffold; (B) represents 20:80 BG/PCL scaffold; and (C) represents 30:70 BG/PCL scaffold.

Fourier Transform Infrared Spectroscopy

FTIR analysis was performed to determine the chemical integrity of scaffold components and their interactions (Fig. 6). In the FTIR spectra, prominent peaks corresponding to Si–O–Si and Si–O–C stretching vibrations were detected, indicating the presence of a silicate network characteristic of BG (Khan *et al.*, 2020). The absorption bands in the region of 400 cm^{-1} to 1,200 cm^{-1} correspond to the Si-O-Si stretching vibrations, while peaks in the region of 800 cm^{-1} to 1,100 cm^{-1} represent Si-O-C stretching vibrations. Additionally, the presence of absorption bands around 600 cm^{-1} to 1,300 cm^{-1} indicates the presence of phosphate (PO_4^{3-}) groups, which are essential components of BG. The absence of peaks in the region of 1,650 cm^{-1} to 1,750 cm^{-1} suggests minimal presence of organic functional groups, indicating high purity of the BG.

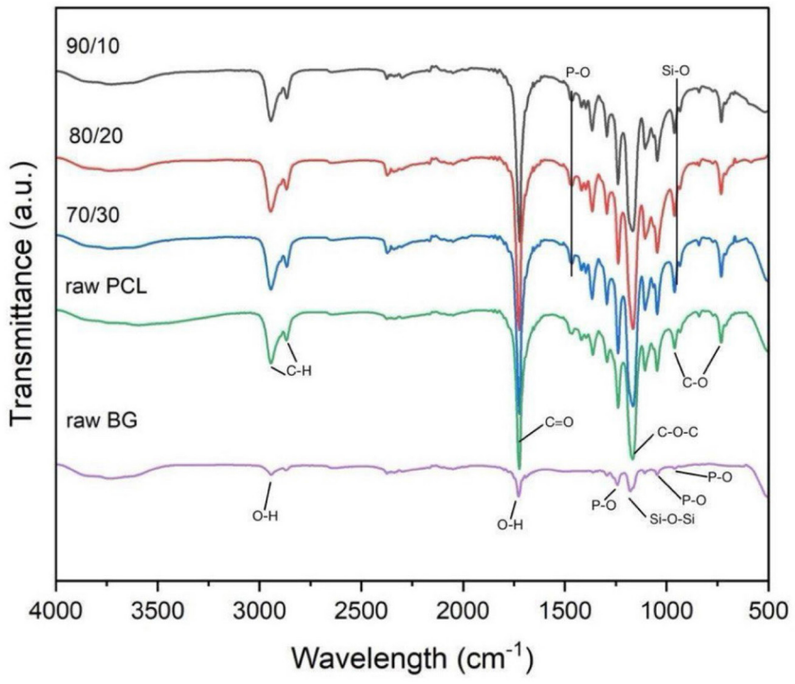

Fig. 6 FTIR graph illustrates the spectra for the pure BG, pure PCL, 10:90, 20:80, and 30:70 BG/PCL scaffold groups.

In contrast to BG, the FTIR spectrum obtained for pure PCL exhibits characteristic absorption bands corresponding to the functional groups present in the polymer. The major peaks observed in the FTIR spectrum typically include stretching vibrations of C=O bonds (carbonyl groups) at around 1,720 cm^{-1}, indicating the presence of ester groups in the PCL polymer chain. Additionally, peaks in the region of 1,150 cm^{-1} to 1,290 cm^{-1} correspond to C-O stretching vibrations, while peaks around 1,400 cm^{-1} to 1,550 cm^{-1} represent stretching vibrations of C-H bonds. The lack of hydroxyl peaks at 3,400 cm^{-1} to 3,500 cm^{-1} confirmed its hydrophobic nature and high purity.

The 10:90 BG/PCL composite spectrum demonstrated successful integration of both phases, preserving key functional groups without new absorption bands, confirmed by BG's silicate/phosphate vibrations coexisting with PCL's carbonyl stretches, though with modified intensities. Peak broadening at 1,000 cm^{-1} to 1,200 cm^{-1} suggested interfacial interactions between Si-O and C-O groups, while the maintained C=O peak position (1,720 cm^{-1}) indicated no ester bond cleavage during fabrication.

Cell Viability Assessment (MTT Assay)

The MTT assay was done to assess cell proliferation and viability on the bone scaffolds of different compositions: 10:90 BG/PCL, 20:80 BG/PCL, and 30:70 BG/PCL, as well as on a control group. Mean absorbance values at 570 nm wavelength were measured as indicators of metabolic activity and cell viability (Fig. 7). HPLF cells cultured on the 10:90 BG/PCL scaffold exhibited a mean absorbance value ranging from > 2.0 to 2.5, indicating robust

metabolic activity and cell proliferation. The relatively high absorbance values suggest a favourable cellular response to the scaffold material. In contrast, cells cultured on the 20:80 BG/PCL scaffold displayed lower mean absorbance values, measuring below 2.0. This suggests a reduction in metabolic activity and cell proliferation compared to the 10:90 BG/PCL scaffold. Although cells were viable on the scaffold, the lower absorbance values indicate a less favourable cellular response compared to the 10:90 BG/PCL scaffold. Similarly, cells cultured on the 30:70 BG/PCL scaffold exhibited mean absorbance values below 2.0, indicating reduced metabolic activity and cell proliferation compared to the 10:90 BG/PCL scaffold. The lower absorbance values suggest a less favourable cellular environment on the 30:70 BG/PCL scaffold, potentially due to differences in scaffold composition and properties. The control group consists of cells without scaffolds, displaying mean absorbance values below 0.5, consistent with baseline metabolic activity levels. This serves as a reference point for assessing the relative impact of scaffold composition on cell viability and proliferation.

The absorbance value for scaffold-only samples was also examined (Fig. 8). Notably, scaffold-only samples exhibited consistent absorbance values, indicating the absence of interference from scaffold compositions on the assay readout. This rigorous powering approach ensures the reliability and reproducibility of the assay results, supporting robust conclusions regarding the biocompatibility and suitability of the scaffold materials for bone tissue engineering applications.

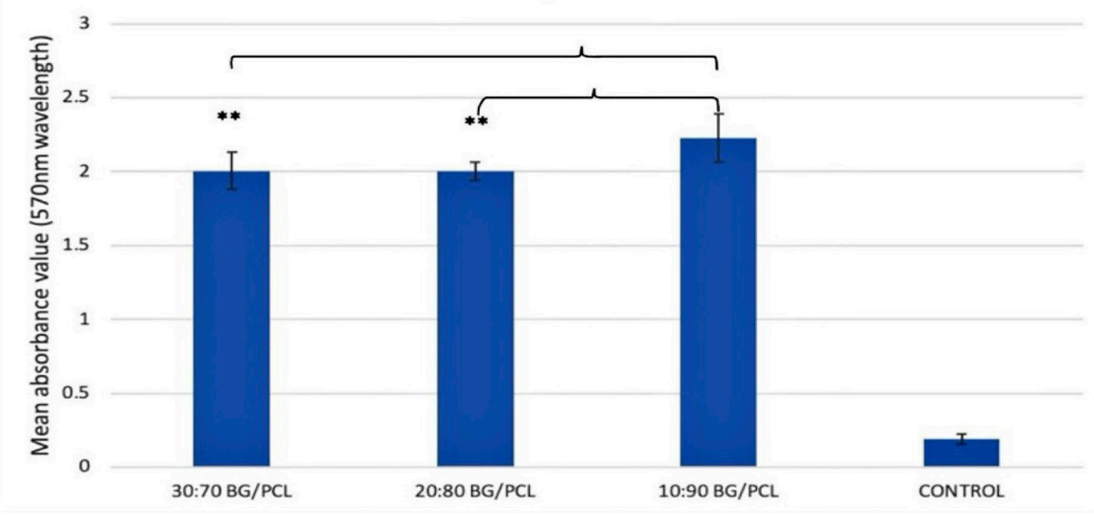

Fig. 7 Bar chart depicting cell viability across various scaffold groups. The x-axis delineates different scaffold compositions, while the y-axis represents the mean absorbance value at 570 nm wavelength, indicative of cellular metabolic activity. **denote $p < 0.001$, indicating highly significant differences specifically between 10:90 and 30:70 scaffold groups, as well as between 20:80 and 10:90 scaffold groups.

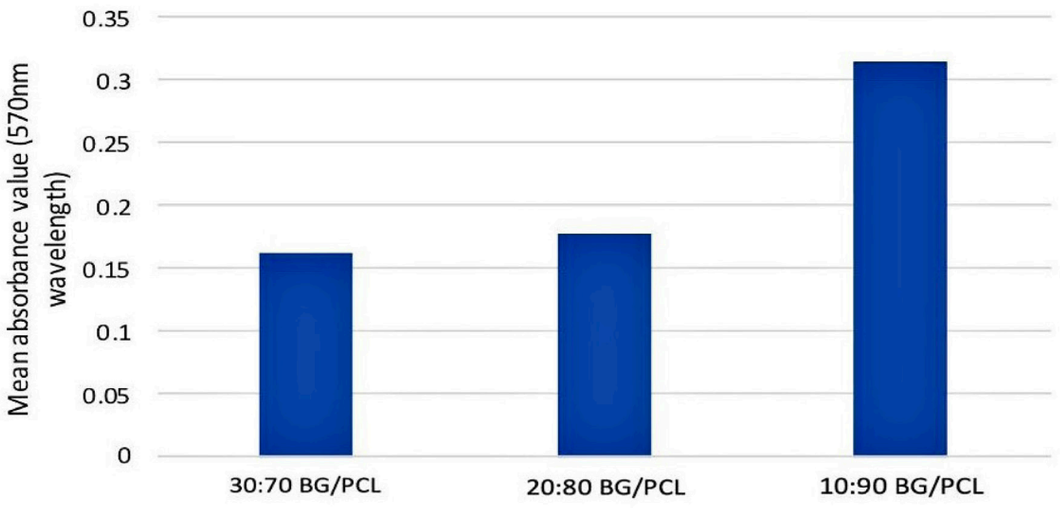

Fig. 8 Bar chart illustrating the absorbance values of scaffolds devoid of cells. The x-axis represents different scaffold compositions, while the y-axis indicates the absorbance values at 570 nm wavelength, reflecting scaffold absorbance independent of cellular metabolic activity.

DISCUSSION

Microarchitecture and Surface Morphology of BG/PCL Scaffold

Analysis of 10:90, 20:80, and 30:70 BG/PCL scaffold structures was carried out using Hitachi TM3000 SEM to determine the microarchitecture, surface morphology, and pore sizes of the samples. The surface roughness of the scaffold observed in Fig. 3 is highly efficient for cell attachment. The pores sizes for each scaffold concentration are also measured (Fig. 4). The pores sizes for each scaffold concentration are also measured. However, even for bone regeneration, no consensus has been determined regarding the optimal pore size in scaffolds, but sufficient porosity of suitable size and interconnections between the pores provides an environment to promote cell infiltration, migration, vascularisation, nutrient and oxygen flow, and waste material removal while being able to withstand external loading stresses (Abbasi *et al.*, 2020). For bone regeneration, pore diameters between 50 and 710 μm have been proposed; numerous studies indicate that macropores between 150 and 350 μm are ideal (Kramschuster & Turng, 2010). Therefore, macropores on the order of hundreds of micrometres with an interconnecting network on the order of tens of micrometres have been identified as ideal for tissue regeneration (Kramschuster & Turng, 2010).

Morphological Analysis of Cell Attachment (SEM)

The observed differences in cell morphology across the three scaffold groups, as depicted under SEM at varying magnifications, provide valuable insights into the interactions between HPLFs and the BG/PCL composite scaffolds. In the 10:90 BG/PCL, numerous clusters of cells were noted under 500× magnification, suggesting cellular aggregation and potential cell-cell interactions within the scaffold microenvironment. At higher magnifications (8,000×), the presence of adherent cells with extended cytoplasmic extensions indicates successful cell adhesion

and spreading, essential for cellular function and tissue integration. Conversely, the 20:80 scaffold group exhibited predominantly elongated and spindle-shaped cells with well-defined cytoplasmic extensions under both magnifications. This morphology is characteristic of healthy cellular adhesion and spreading, signifying favourable interactions between HPLFs and the scaffold surface. Notably, the 30:70 BG/PCL displayed fewer cell clusters under 500× magnification compared to the other groups, suggesting a less conducive microenvironment for cellular aggregation. However, examination at 8,000× magnification revealed adherent cells with elongated extensions, akin to those observed in the other groups. These findings suggest that despite variations in cell aggregation at lower magnifications, all scaffold groups ultimately support cellular adhesion and spreading, essential for tissue regeneration. The observed differences in cell morphology may be attributed to variations in scaffold composition and surface characteristics.

Fourier Transform Infrared Spectroscopy

The FTIR spectra obtained for the BG/PCL scaffolds revealed characteristic absorption bands corresponding to the functional groups present in the PCL and BG components. The spectra were compared to those of raw PCL and raw BG to assess the influence of scaffold composition on chemical bonding and interactions.

The results of FTIR measurements on the BG/PCL scaffolds are shown (Fig. 6). Obtained FTIR spectra also indicate the interatomic bindings in BG structure. The characteristic bonds at 1,178.7 cm^{-1} is related to bending and stretching bonds of Si-O-Si. Characteristic band at 926 cm^{-1} is related to stretching bond of Si-O and characteristic bands at 626.4 and 1,242.4 cm^{-1} are related to P-O bonds. These peaks serve as reference points for identifying the presence of BG in the scaffold samples comparable to a study by Sadeghinia *et al.* (2021).

Similarly, the FTIR spectra of raw BG displayed characteristic absorption bands corresponding to the functional groups present in BG, such as characteristic peaks at 731.3 and 934.4 cm^{-1} are related to C-O bonds, peaks at 1,045.3 cm^{-1}, 1,167.7 cm^{-1} and 1,239.7 cm^{-1} are attributed to C-O-C stretching bonds of PCL while stretching vibration bands in wavenumber range of 1,418.5cm^{-1} to 1,510.5 cm^{-1} are related to C-H bond. Band at 1,721.8 cm^{-1} related to stretching bond of carbonyl C=O in PCL, while peaks with wave numbers of 2,866.6 cm^{-1} and 2,944.0 cm^{-1} belong to stretching bonds of C-H in PCL. These peaks are comparable to a study by Sadeghinia *et al.* (2021).

Upon comparing the FTIR spectra of the BG/PCL scaffolds to those of raw PCL and raw BG, differences in peak intensities and positions were observed, indicative of chemical interactions between the polymer and BG components. For example, shifts in peak positions or changes in peak intensities suggest the formation of new chemical bonds or interactions between functional groups within the scaffold matrix (Hooi *et al.*, 2021).

The FTIR spectra of the BG/PCL scaffolds exhibited peaks corresponding to both PCL and BG functional groups, suggesting the presence of both components in the scaffold compositions. Additionally, variations in peak intensities and shapes were observed among the different scaffold compositions, indicating differences in chemical bonding and interactions.

For instance, the presence of FTIR peaks corresponding to both PCL and BG in the 10:90 scaffold confirms the successful incorporation of both materials within the composite matrix, with relatively high intensities compared to the other compositions. This suggests strong interactions between the polymer and BG components, potentially leading to enhanced scaffold stability and bioactivity (Sadeghinia *et al.*, 2021).

Cell Viability Assessment (MTT Assay)

The MTT assay results provide valuable insights into the biocompatibility and cytocompatibility of BG/PCL composite scaffolds with human periodontal ligament fibroblasts (HPLFs). The favourable viability and metabolic activity of PDL fibroblasts on all three scaffold compositions (10:90, 20:80, and 30:70 BG/PCL) indicate the scaffolds' ability to support cell growth and proliferation. Among the three compositions, the 10:90 BG/PCL scaffold showed the greatest cell viability, with progressively lower values observed for the 20:80 and 30:70 groups.

The observed differences in cell viability could be attributed to various scaffold characteristics, including porosity and surface roughness. SEM analysis revealed that the 10:90 BG/PCL scaffold exhibited the largest and most well-defined pore structures, potentially providing a favourable environment for cell attachment and proliferation. In contrast, the 30:70 BG/PCL scaffold demonstrated the lowest porosity, which may have limited cell infiltration and nutrient exchange within the scaffold matrix (Abbasi *et al*., 2020).

Furthermore, scaffold surface roughness is known to influence cellular responses, with rougher surfaces promoting enhanced cell adhesion and metabolic activity. The 10:90 BG/PCL scaffold, characterised by higher surface roughness, may have facilitated better cell-scaffold interactions compared to the smoother surfaces of the 20:80 BG/PCL and 30:70 BG/PCL scaffolds.

The BG component in the scaffolds also likely contributed to their bioactivity and osteogenic potential. While the 10:90 BG/PCL scaffold contained the lowest proportion of BG, its bioactive properties may have been sufficient to stimulate favourable cellular responses. It suggests complex interactions between scaffold composition, microstructure, and cell behaviour.

The findings of this study underscore the importance of comprehensive scaffold characterisation and optimisation in tissue engineering applications. Scaffold design parameters, including composition, microstructure, and surface properties, play critical roles in determining cellular behaviour and ultimately, the success of scaffold-cell interaction in regenerating new bone tissue.

CONCLUSION

In this study, it was revealed that among the tested compositions, the 10:90 BG/PCL scaffold exhibited the most promising features across multiple parameters. Based on all tests and analyses that have been done, it demonstrated that the 10:90 BG/PCL scaffold possessed the highest surface roughness, largest pore sizes, highly crystalline material, and highest cell viability percentage, indicative of its excellent cytocompatibility and potential for tissue regeneration. In conclusion, our evaluation indicates that the 10:90 BG/PCL scaffold possesses an optimal combination of surface roughness, porosity, and biocompatibility, highlighting its potential as a promising candidate for subsequent stages of our research, including the *in vivo* and *in vitro* analysis. Its applicability for those mentioned above proposed additional analyses, highlighting its capacity to greatly advance our knowledge of scaffold performance and its practical applications in tissue engineering and regenerative medicine.

ACKNOWLEDGEMENTS

We are grateful for the access to the laboratories, research materials, and technological resources offered by the Faculty of Dentistry, Universiti Teknologi MARA (UiTM) Sungai Buloh and Faculty of Applied Science, UiTM Shah Alam. These resources have been instrumental in conducting experiments, gathering data,

and analysing findings. Lastly, we are immensely grateful to all the individuals who contributed to this research collaboration. The dedication, expertise, and unwavering support have been instrumental in achieving our research goals.

REFERENCES

Abay A, Simionato G, Chachanidze R, Bogdanova A, Hertz L, Bianchi P *et al.* (2019). Glutaraldehyde – A subtle tool in the investigation of healthy and pathologic red blood cells. *Front Physiol*, **10**: 514. https://doi.org/10.3389/fphys.2019.00514

Abbasi N, Hamlet S, Love RM, Nguyen NT (2020). Porous scaffolds for bone regeneration. *J Sci Adv Mater Devices*, **5**(1): 1–9. https://doi.org/10.1016/j.jsamd.2020.01.007

Darie-Niţă RN, Rapa M, Frackowiak S (2022). Special features of polyester-based materials for medical applications. *Polymers*, **14**(5): 951. https://doi.org/10.3390/polym14050951

Ghassemi T, Shahroodi A, Ebrahimzadeh MH, Mousavian A, Movaffagh J, Moradi A (2018). Current concepts in scaffolding for bone tissue engineering. *Arch Bone Jt Surg*, **6**(2): 90–99.

Granel H, Bossard C, Collignon A-M, Wauquier F, Lesieur J, Rochefort GY *et al.* (2019). Bioactive glass/polycaprolactone hybrid with a dual cortical/trabecular structure for bone regeneration. *ACS Appl Bio Mater*, **2**(8): 3473–3483. https://doi.org/10.1021/acsabm.9b00407

Hooi MT, Phang ESW, Yow HY, David E (2021). FTIR spectroscopy characterization and critical comparison of poly(vinyl) alcohol and natural hydroxyapatite derived from fish bone composite for bone-scaffold. *J Phys Conf Ser*, **2120**: 012004. https://doi.org/10.1088/1742-6596/2120/1/012004

Khan MUA, Mehboob H, Abd Razak SI, Yahya MY, Mohd Yusof AH, Ramlee MH *et al.* (2020). Development of polymeric nanocomposite (xyloglucan-co-methacrylic acid/hydroxyapatite/SiO_2) scaffold for bone tissue engineering applications—in-vitro antibacterial, cytotoxicity and cell culture evaluation. *Polymers*, **12**(6): 1238. https://doi.org/10.3390/polym12061238

Kramschuster A, Turng LS (2010). An injection molding process for manufacturing highly porous and interconnected biodegradable polymer matrices for use as tissue engineering scaffolds. *J Biomed Mater Res B Appl Biomater*, **92**(2): 366–376. https://doi.org/10.1002/jbm.b.31523

Kundu J, Shim JH, Jang J, Kim SW, Cho DW (2015). An additive manufacturing-based PCL-alginate-chondrocyte bioprinted scaffold for cartilage tissue engineering. *J Tissue Eng Regen Med*, **9**(11): 1286–1297. https://doi.org/10.1002/term.1682

Kuo C-K, Huang H-W, Chen L-G, Chou Y-J (2021). Fabrication and characterization of freeze-dried strontium-doped bioactive glasses/chitosan composite scaffolds for biomedical engineering. *J Asian Ceram Soc*, **9**(3): 1173–1182. https://doi.org/10.1080/21870764.2021.1946269

Larsson L, Decker AM, Nibali L, Pilipchuk SP, Berglundh T, Giannobile WV (2016). Regenerative medicine for periodontal and peri-implant diseases. *J Dent Res*, **95**(3): 255–266. https://doi.org/10.1177/0022034515618887

Lu L, Zhang Q, Wootton DM, Chiou R, Li D, Lu B *et al.* (2014). Mechanical study of polycaprolactone-hydroxyapatite porous scaffolds created by porogen-based solid freeform fabrication method. *J Appl Biomater Funct Mater*, **12**(3): 145–154. https://doi.org/10.5301/jabfm.5000163

Malagón-Escandón A, Hautefeuille M, Jimenez-Díaz E, Arenas-Alatorre J, Saniger JM, Badillo-Ramírez I *et al.* (2021). Threedimensional porous scaffolds derived from bovine cancellous bone matrix promote osteoinduction, osteoconduction, and osteogenesis. *Polymers*, **13**(24): 4390. https://doi.org/10.3390/polym13244390

Manodh P, Prabhu Shankar D, Pradeep D, Santhosh R, Murugan A (2016). Incidence and patterns of maxillofacial trauma—a retrospective analysis of 3611 patients—an update. *Oral Maxillofac Surg*, **20**(4): 377–383. https://doi.org/10.1007/s10006-016-0576-z

Muzaffar J, Bari S, Kirtane K, Chung CH (2021). Recent advances and future directions in clinical management of head and neck squamous cell carcinoma. *Cancers*, **13**(2): 338. https://doi.org/10.3390/cancers13020338

Nanci A, Bosshardt DD (2006). Structure of periodontal tissues in health and disease. *Periodontol 2000*, **40**(1): 11–28. https://doi.org/10.1111/j.1600-0757.2005.00141.x

Sadeghinia Z, Emadi R, Shamoradi F (2021). A study of the electrophoretic deposition of polycaprolactone-chitosan-bioactive glass nanocomposite coating on stainless steel (316L) substrates. *J Bioact Compat Polym*, **37**(1): 53–71. https://doi.org/10.1177/08839115211063506

Safi IN, Al-Shammari AM, Ul-Jabbar MA, Hussein BMA (2020). Preparing polycaprolactone scaffolds using electrospinning technique for construction of artificial periodontal ligament tissue. *J Taibah Univ Med Sci*, **15**(5): 363–373. https://doi.org/10.1016/j.jtumed.2020.07.007

Ufere SKJ, Sultana N (2016). Fabrication and characterization of PCL/HA/PPY composite scaffold using freezedrying technique. *J Teknol*, **78**(12): 89–94. https://doi.org/10.11113/jt.v78.10072

Wusiman P, Maimaitituerxun B, Guli, Saimaiti A, Moming A (2020). Epidemiology and pattern of oral and maxillofacial trauma. *J Craniofac Surg*, **31**(5): e517–e520. https://doi.org/10.1097/SCS.0000000000006719

Yousefiasl S, Sharifi E, Salehinejad E, Makvandi P, Irani S (2023). Bioactive 3D-printed chitosan-based scaffolds for personalized craniofacial bone tissue engineering. *Eng Regen*, **4**(1): 1–11. https://doi.org/10.1016/j.engreg.2022.09.005